Synthetic Phase Contrast Imaging Diagnostic for Wendelstein 7-X

S.K. Hansen[1], M. Porkolab[1], Z. Huang[1], J.-P. Bähner[2], A. von Stechow[2], O. Grulke[2,3], E.M. Edlund[4], A. Bañón Navarro[5], E. Sánchez[6], and the Wendelstein 7-X Team

[1] *Plasma Science and Fusion Center, MIT, Cambridge, MA 02139, USA*

[2] *Max-Planck-Institut für Plasmaphysik, 17491 Greifswald, Germany*

[3] *Department of Physics, Technical University of Denmark, 2800 Kgs. Lyngby, Denmark*

[4] *State University of New York College at Cortland, Cortland, NY 13045, USA*

[5] *Max-Planck-Institut für Plasmaphysik, 85748 Garching, Germany*

[6] *Laboratorio Nacional de Fusión, CIEMAT, 28040 Madrid, Spain*

We describe early results from the synthetic phase contrast imaging (PCI) diagnostic developed for the optimized stellarator Wendelstein 7-X (W7-X). The PCI system is the main core turbulence diagnostic at W7-X [1] and the focus of the synthetic diagnostic development has therefore been on computing PCI signals from turbulent fluctuating electron density, $\tilde{n}_e$, profiles, modeled using the nonlinear, global gyrokinetic codes EUTERPE [2] and GENE-3D [3].

Figure 1 shows the essential elements of the W7-X PCI system modeled within the synthetic diagnostic. A collimated CO_2 laser beam with electric field profile $\mathbf{E}_0$ is injected. Upon passing the plasma, the beam profile is modified to $\mathbf{E}_{\rm obj}$. The effect of the plasma on the laser beam, which is relevant to PCI, may be described by the fluctuating phase shift along a line-of-sight (LoS), $\tilde{\phi} = -r_e\lambda_0 \int_{\rm LoS} \tilde{n}_e \,{\rm d}z \ll 1$, where $r_e = 2.81794$ fm is the classical electron radius and $\lambda_0 = 10.6\,\mu$m (at W7-X [1]) is the vacuum wavelength of the laser [4],

$$\mathbf{E}_{\rm obj} = \mathbf{E}_0 {\rm e}^{{\rm i}\tilde{\phi}} \approx \mathbf{E}_0(1+{\rm i}\tilde{\phi}). \tag{1}$$

The approximation in Eq. (1) shows that the beam may be considered to consist of an unscattered part, characterized by the 1, and a (small-angle) scattered part, characterized by the ${\rm i}\tilde{\phi}$, within the Born approximation [4]. The scattered and uscattered parts of the beam are separated in the focal plane of a mirror, as seen in Fig. 1. If a phase plate, which is a mirror containing a central groove of depth $\lambda_0/8$ and width $d = 1.1$ mm (at W7-X [1]), also seen in Fig. 1, is placed in the focal plane of the mirror, it is possible to impart an extra phase shift of $\pi/2$ to the unscattered part of the beam. Further taking into account that the central groove of the mirror has a reduced reflection coefficient, $R = 0.28$ (at W7-X [1]), and accounting for the magnification of the PCI system, M, the electric field and intensity of the beam in the image plane, $\mathbf{E}_{\rm im}$ and $I_{\rm im}$, respectively, may be expressed as

$$\mathbf{E}_{\rm im}(x/M) = M\mathbf{E}_0({\rm i}\sqrt{R}+{\rm i}\tilde{\phi}) \;\Rightarrow\; I_{\rm im}(x/M) = \frac{|\mathbf{E}_{\rm im}(x/M)|^2}{2\eta_0} \approx \frac{M^2|\mathbf{E}_0|^2(R+2\sqrt{R}\tilde{\phi})}{2\eta_0}, \tag{2}$$

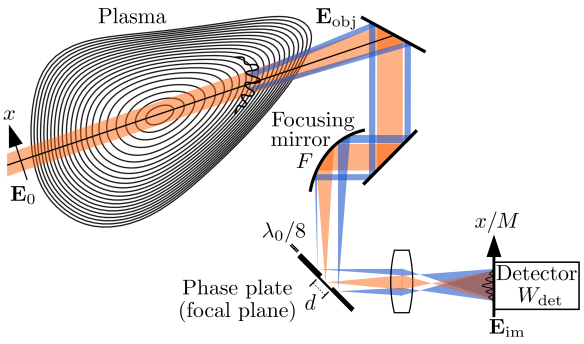

Figure 1: Schematic of the synthetic PCI model implemented at W7-X.

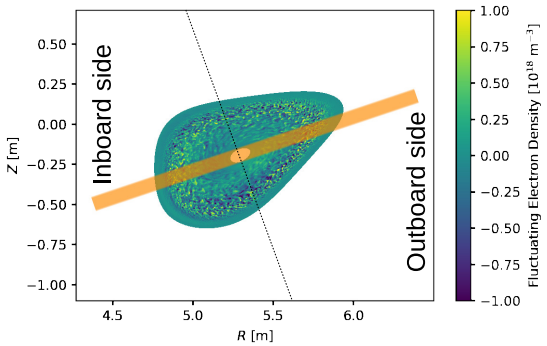

Figure 2: PCI LoSs superimposed on an $\tilde{n}_e$ field from the GENE-3D simulation [3].

where x is the direction transverse to the beam in the plasma seen in Fig. 1 and $\eta_0 = 376.73\ \Omega$ is the impedance of free space. Equation (2) shows that the presence of the phase plate in the focal plane converts the phase modulation in the object plane into an amplitude modulation in the image plane, allowing $\tilde{\phi}$ to be imaged by a detector array, consisting of 32 square HgCdTe elements of width, $W_{\text{det}} = 0.5$ mm, cooled by liquid nitrogen at W7-X [1]; the reduced R of the central groove of the phase plate improves the signal-to-noise ratio [1, 4]. The requirement that the scattered part of the beam should not hit the groove of the phase plate imposes a minimum wave number along the x-direction, k, which must be exceeded in order for the fluctuations to be imaged by PCI [4], $k_{\text{min}} = \pi d/(F\lambda_0) = 1.6\,\text{cm}^{-1}$ (at W7-X), where $F = 2.032$ m (at W7-X [1]) is the focal length of the mirror. This effect is quantified by implementing the PCI instrument response of [4] in the synthetic diagnostic. To compute the PCI signal, I_{im} is integrated over each detector element and multiplied by a detector response, taken to be 6 kV/W for the detector elements used at W7-X [5]. The integration over the detector elements further introduces an upper limit on the k that may be imaged by the Nyquist wave number, $k_{\text{max}} = \pi/(W_{\text{det}}M) = 62.8\,\text{cm}^{-1}/M$ (at W7-X). The synthetic PCI diagnostic is implemented in similar manner for the EUTERPE [2] and GENE-3D [3] simulations. First, a time series of $\tilde{n}_e$ is extracted from the simulations on a rectangular grid in straight field line coordinates around the toroidal location of the PCI LoSs; a slice of $\tilde{n}_e$ from the GENE-3D simulation in cylindrical coordinates is seen in Fig. 2. Then, the coordinates of the LoSs (also seen in Fig. 2) are computed in straight field line coordinates, $\tilde{n}_e$ is interpolated to the LoSs, and a direct image of $\tilde{\phi}$ is computed through numerical integration. Finally, the PCI signal is computed by integrating I_{im} over the the detector elements and multiplication by the detector response of 6 kV/W [5].

The PCI signal obtained from the EUTERPE simulation with $M = 5$, along with the wave number-frequency (k, f) spectra obtained based on it, is seen in Fig. 3. The top row of Fig. 3

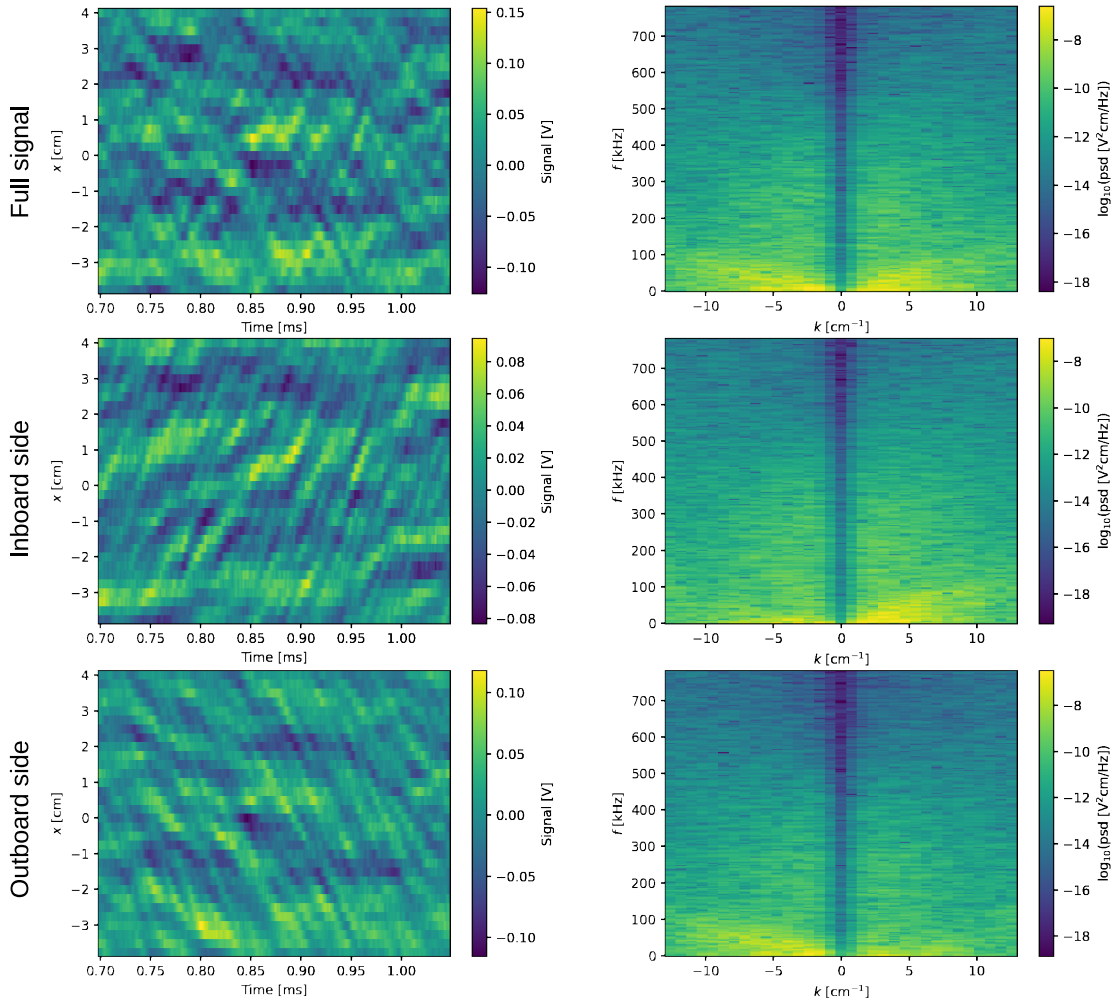

Figure 3: Synthetic PCI signals (left column) and (k, f) spectra (right column) from the EUTERPE simulation [2]. The top row shows the result obtained when $\tilde{n}_e$ is integrated over the full LoS, while the middle and bottom rows show the results obtained from integration over the inboard and outboard sides, respectively.

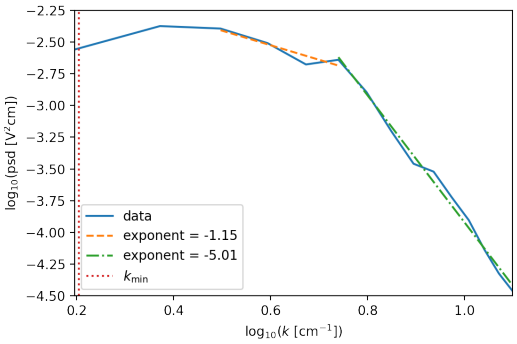

Figure 4: Synthetic PCI k spectrum based on the EUTERPE simulation [2].

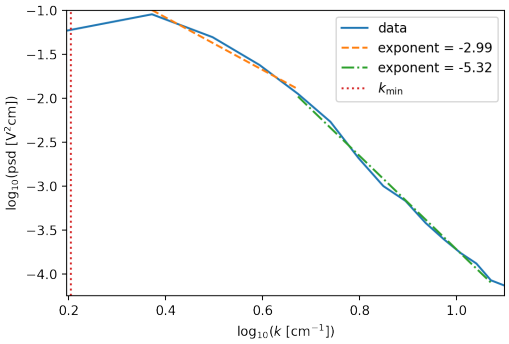

Figure 5: Synthetic PCI k spectrum based on the GENE-3D simulation [3].

shows the signal and (k, f) spectrum obtained from integration over the full LoS. It indicates that structures propagating along both the positive and negative x-direction exist in the plasma; the low-k cutoff imposed by the PCI system is also visible in the (k, f) spectrum. For interpreting the rotation direction, the middle and lower rows, respectively showing the signals and (k, f) spectra obtained from integration over the inboard and outboard sides, as defined in Fig. 2, are of more interest. On the inboard side, the structures primarily propagate in the positive x-direction, while they propagate in the negative x-direction on the outboard side, corresponding to rotation in the electron diamagnetic direction. This is opposite to that of linear ion temperature gradient modes, which dominate both simulations due to the use of adiabatic electrons [2, 3], but we note that the rotation in the simulations is dominated by zonal flows, whose direction is determined by nonlinear effects; neither simulation includes a neoclassical radial electric field, E_r, which dominates the experimental rotation [6]. We also note that the signal from the outboard side is stronger than that from the inboard side, as generally expected in toroidal devices. To gain more basic information about the turbulence, we compute k spectra, by integrating the (k, f) spectra over f, for the EUTERPE and GENE-3D simulations in Figs. 4 and 5, respectively. In both cases, the spectral power decreases according to a power law with an exponent close to -5 for sufficiently large k, in agreement with expectations for electrostatic drift wave turbulence [7], indicating that interchange-like modes may be of limited importance. Finally, a neoclassical E_r may be superimposed on the simulations to mimic experimental PCI signals [6].

Acknowledgments

SKH was supported by an Internationalisation Fellowship (CF19-0738) from the Carlsberg Foundation. Support for the MIT and SUNY-Cortland participation was provided by the US Department of Energy, Grant DE-SC0014229. This work has been carried out within the framework of the EUROfusion Consortium and has received funding from the Euratom research and training programme 2014−2018 and 2019−2020 under grant agreement No. 633053. The views and opinions expressed herein do not necessarily reflect those of the European Commission.

References

[1] Z. Huang et al., *J. Instrum.* **16**, P01014 (2021)

[2] E. Sánchez et al., *J. Plasma Phys.* **86**, 855860501 (2020)

[3] A. Bañón Navarro et al., *Plasma Phys. Control. Fusion* **62**, 105005 (2020)

[4] S. Coda, *Ph.D. Thesis* (MIT, Cambridge, 1997)

[5] http://www.teledynejudson.com/products/photoconductive-mercury-cadmium-telluride-detectors

[6] J.-P. Bähner et al., *J. Plasma Phys.* (accepted) (2021)

[7] C.M. Tchen, H.L. Pécseli, and S.E. Larsen, *Plasma Phys.* **22**, 817 (1980)